Areas of Opportunity Related to Design of Chemical and Biological Sensors based on Liquid Crystals.

Karthik Nayani[1,2], Yu Yang[1], Huaizhe Yu[1], Purvil Jani,[1] Manos Mavrikakis[3] and Nicholas Abbott[1]

[1]School of Chemical and Biomolecular Engineering, Cornell University, Ithaca NY, 14853

[2]Department of Chemical Engineering, University of Arkansas, Fayetteville, AR, 72701

[3]Department of Chemical and Biological Engineering, University of Wisconsin, Madison WI 53706

Abstract. The large societal impact of liquid crystals (LCs) in electrooptical displays arrived after several decades of research involving molecular-level design of LCs and their alignment layers, and elucidation of LC electrooptical phenomena at device scales. The unusual anisotropic optical, mechanical and dielectric properties of LCs used in displays also makes LCs remarkable amplifiers of their interactions with chemical and biological species, thus opening up the possibility that LCs may play an equally influential role in a data-driven society that increasingly depends on information coming from sensors. In this article, we briefly describe ongoing efforts to design LC systems tailored for chemical and biological sensing, efforts that in many ways mirror the challenges and opportunities in LC design and alignment tackled several decades ago during development of LC electrooptical displays. Now, however, traditional design approaches based on structure-property relationships are being supplemented by data-driven methods such as machine learning. Recent studies also show that computational chemistry methods can greatly increase the rate of discovery of chemically-responsive LC systems. Additionally, non-equilibrium states of LCs are being revealed to be useful for design of biological sensors and more complex autonomous systems that integrate self-regulated actuation along with sensing. These topics and others are briefly addressed in this article with the aim of highlighting approaches and goals for future research that will realize the full potential of LC-based sensors.

Introduction. The idea of creating chemical and biological sensors that exploit the properties of liquid crystals (LCs) is not new. Before mankind roamed the surface of Earth, evolutionary processes selected the liquid crystalline state of matter as the basis of life[1, 2], because LCs can reorganize in response to subtle chemical and mechanical cues to perform useful functions[2] (e.g., as underlies the functioning of a mammalian cell membrane). A bit more recently, and in parallel and following the development of liquid crystal displays in the 1970's[3], a range of studies have explored the properties of synthetic LCs as the basis of chemical and biological sensors[4-16]. In the year 2020, as societal challenges such as management of COVID-19, global changes in climate, and creation of a circular economy, have moved to the front-burner, the pull for innovation and translation of sensing technologies is strong: data acquisition and analysis are central elements of decision-making common to all of these challenges, and sensors, in many cases, are the source of that data. For the research community with expertise in LCs, the opportunity to have an impact is being amplified by the emergence of new tools for LC bio/chemical sensor design, including

electronic-structure calculations and AI techniques. This brief perspective aims to convey select opportunities connected to LC sensor design, with a focus on approaches enabled by new scientific tools and methodologies.

Chemical Sensors Create the Need for New LC Alignment Chemistries and Mesogen Designs. The development of stable and long-lived surface chemistries for alignment of LCs, such as is achieved via use of surfaces coated with polyimides, underlies the success of the electrooptical LC display technology[3]. One broad class of strategies for the design of LC chemical sensors aims to build from this success by creating tailored surfaces that cause LCs to change orientation in the presence of a targeted chemical species (Figure 1a)[10, 12, 16-21]. Approaches used to date to transduce and quantify surface-driven changes in the orientation of LCs in sensors include measurement of light transmitted through polarizers, absorbance of guest-host systems, and electrical capacitance. In contrast to displays, however, in addition to the solid-LC interface, a LC chemical or biological sensor must have a free surface, either to the atmosphere for gas sensing[22] or an aqueous phase for sensing of biological species in water[23]. These unconventional interfaces in LC sensors create additional challenges and opportunity for fundamental science and technological contribution. Here we focus on recent efforts to address these issues, with the goal of sending the message that opportunities exist both for surface chemists and those skilled in the synthesis of new LCs to make important contributions.

The degrees of freedom underlying the design of surfaces and LCs for surface-driven LC sensors is large, leading to the

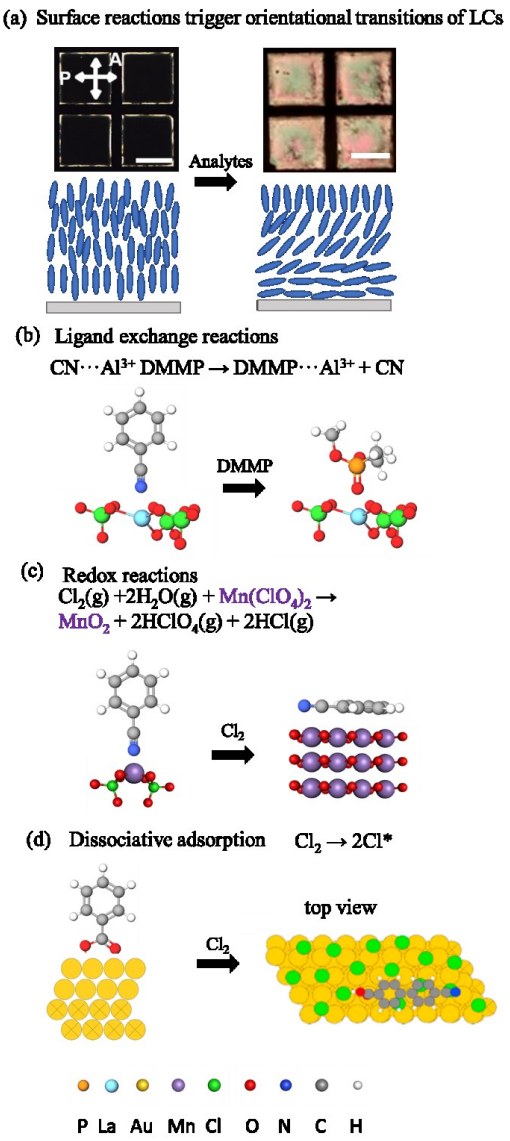

Figure 1. Design of reactive surfaces for LC chemical sensors. (a) General design principle: the optical response of the LC sensor is triggered by a surface anchoring transition. Surface anchoring transitions in LC sensors have been triggered by (b) metal cation-ligand exchange reactions (e.g., exchange of nitrile group of mesogen with phosphoryl group of DMMP) (c) redox reactions (oxidation of Mn^{2+} to Mn^{4+} (as MnO_2) by Cl_2 in the presence of water vapor) and (d) reactions on noble metal surfaces (dissociative adsorption of Cl_2 displacing mesogen bound to Au(111)). From references[19, 21].

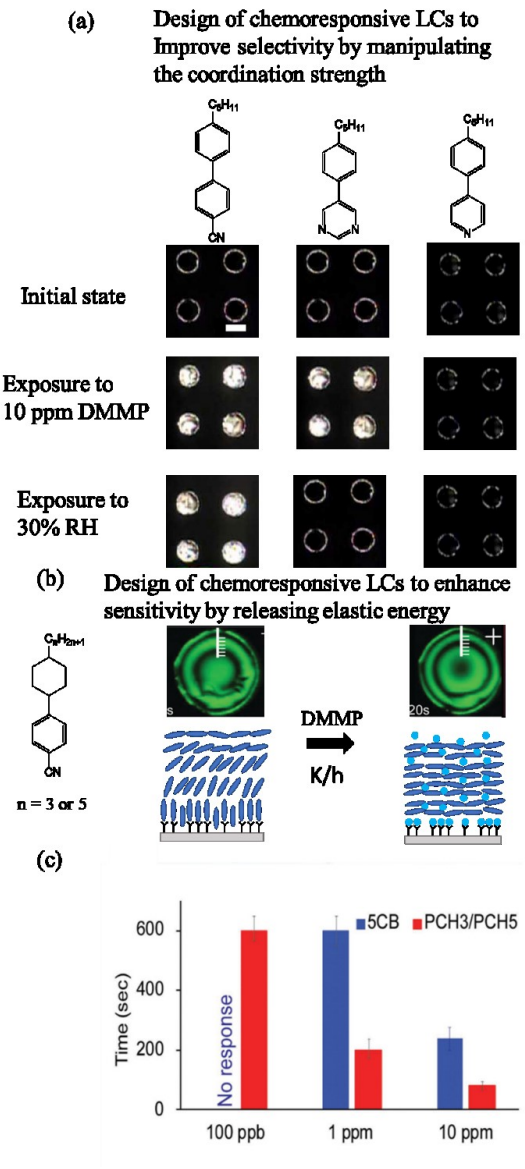

Figure 2. Design of LCs tailored for use in sensors. (a) Optical micrographs (crossed polars) of LCs comprised of pure 5CB, 5CB with a pyrimidine-based dopant, or 5CB containing a pyridine-based dopant, supported on surfaces decorated with Al^{3+} : initial state, exposed to a vapor of 10 ppm DMMP in nitrogen, and exposed to a vapor of 30% relative humidity of nitrogen. (b) Time-dependent change in interference fringes of PCH3/PCH5 mixture supported on La^{3+} decorated surface, following introduction of DMMP (10 ppm). The ruler indicates the change in fringe position. (c) Characteristic time to achieve an 80% response for PCH3/PCH5 and 5CB as a function of DMMP concentration. From reference [22, 27].

need to optimize multiple design parameters. Significantly, recent studies have demonstrated that computational chemistry techniques can be used to screen select degrees of freedom to identify suitable LCs and reactive surfaces for a given chemical target, as described below. The first design of a LC surface-driven sensor that we introduce here is inspired by classical observations of adsorbate-triggered anchoring transitions[24], in which changes in the intermolecular interaction between a LC and the surface of a solid leads to an alteration of the easy axis/anchoring energy of the LC[12, 17, 25]. We illustrate the approach using surfaces that present metal cation binding sites, and LCs that possess functional groups (e.g., nitrile groups) that participate in coordination interactions with select metal cations[12]. For a LC such as nematic 4'-pentyl-4-biphenylcarbonitrile (5CB), the formation of a coordination complex of sufficient strength at the metal ion-decorated solid surface leads to a uniform homeotropic orientation of the LC[26]. This interpretation of experiments is supported by computations of the binding energies of benzonitrile for metal cations[18, 20, 21, 27]. An anchoring transition of the LC is triggered by exposure of the free surface of the oriented LC film to gaseous species that diffuse through the LC film and bind to the metal cation more strongly than the mesogens of the LC. A widely explored example (Figure 1b) of gaseous species that will trigger this type of anchoring transition is the organophosphonate class of compounds (relevant to pesticides and chemical warfare agents), such as dimethylmethylphosphonate (DMMP). Consistent with experimental observations of anchoring transitions triggered by DMMP and nerve agents, electronic structure calculations predict that the binding energy of DMMP to Al^{3+} (-1.14 eV) is stronger than that of 5CB to Al^{3+} (-0.40 eV) and thus that the orientational

transition of 5CB is driven by ligand exchange at the surface (nitrile of 5CB by phosphoryl of DMMP)[18, 20, 21, 27]. Experiments demonstrate that this experimental design can be highly sensitive; for example, parts-per-billion concentrations of DMMP in the gas phase can trigger anchoring transitions of 5CB supported on Al^{3+} functionalized surfaces[19, 25]. Through judicious selection of the metal cation, its counter ions, and the ligands incorporated into mesogens, a wide range of chemically specific LC systems can be created [18-21, 25, 27]. Here again, computational chemistry methods are proving increasingly useful in screening these degrees of freedom.

A second strategy for the design of chemically responsive interfaces for use in LC sensors relies on interfacial redox reactions. This strategy works well for oxidizing and reducing gases that, for example, bind weakly with metal cations and thus cannot be detected using the strategy described above. As an example of this strategy (Figure 1c), we describe the use of surfaces presenting Mn^{2+} cations and detection of Cl_2 gas (an oxidizing gas) [19]. Whereas nitrile-containing LCs bind strongly to Mn^{2+} binding sites on surfaces, exposure of Mn^{2+}-decorated surfaces to humid (35% relative humidity) Cl_2 gas triggers a redox reaction that results in formation of Mn^{4+} (in the form of MnO_2), which in turn triggers a change in the orientation of the supported LC from homeotropic to planar. Interestingly, the orientations of the LC before and after the redox-reaction were predicted by electronic structure calculations [19], again highlighting the opportunity to use computational chemistry to guide the design of new types of LC chemical sensors. In contrast to the metal ligand-exchange reactions outlined above, the oxidation of the Mn^{2+} to MnO_2 is irreversible, and thus is suitable for one-time alarm sensors or sensors that report cumulative exposure, as is needed for quantification of chronic human exposure to chemical environments. The selectivity of the sensor can be tuned via choice of the mesogen and metal cation with its associated anion (or other redox species), thus creating a substantial (and largely unexplored) design space.

The third surface-based strategy for design of LC sensors that we outline here revolves around reactive surfaces. We illustrate this design by describing the use of a noble metal surface to anchor a LC (Figure 1d)[21]. While many LCs (e.g., cyanobiphenyls) are known to orient parallel to the surfaces of noble metal surfaces such as the Au(111) surface, substantial research in the field of heterogeneous catalysis reveals that a range of chemical functional groups undergo chemical transformations on these surfaces. For example, aromatic carboxylic acids will undergo a dehydrogenation reaction on Au(111), resulting in directional binding[28]. Guided by these prior results, aromatic carboxylic acids have been used recently as dopants in cyanobiphenyl-based LCs and shown to cause the LCs to adopt a homeotropic orientation as a consequence of dehydrogenation of the carboxylic group of the dopant[21]. Complementary computations confirmed the experimental observations, but also predicted that dissociative adsorption of Cl_2 gas on the Au(111) surface would displace the bound (dehydrogenated) carboxylic acid. This prediction was validated by experiment, revealing that subsequent exposure of the LC system to Cl_2 gas triggered an anchoring transition due to dissociative adsorption of Cl_2 gas to atomic Cl on the Au(111) surface (Figure 1d). This design of a LC sensor for Cl_2 was shown to be robust and tolerant to many other chemical species and, more broadly, serves to highlight the opportunity to leverage knowledge from the field of surface science and heterogeneous catalysis to advance the design of LC sensors.

In each of the approaches described above, there exists a largely untapped opportunity to refine the sensitivity and specificity of LC sensors via optimization of the structure of the mesogens and properties of the LC phase[21, 22, 27]. For example, whereas many past studies of LC sensors have used the cyanobiphenyl series of LCs, dopants and mesogens that contain pyridine and pyrimidine groups have been shown to yield substantial improvements in terms of chemical selectivity of the sensors (i.e., responding to one chemical species but not another)[27]. We illustrate the opportunity to create new mesogens with properties tailored for LC sensors with an example that was informed by the use of computational chemistry. In the example shown in Figure 2a, as predicted by binding energies from electronic structure computations, LCs containing nitrile groups bind to Al^{3+} cations on surfaces more weakly (-0.40 eV) than DMMP (-1.14 eV) or water (-0.49 eV), and thus nematic 5CB undergoes a surface-driven anchoring transition in response to DMMP or water. In contrast, LCs containing pyridine groups bind too strongly to the Al^{3+}-decorated surfaces to respond to either DMMP or water, whereas LCs containing pyrimidine groups bind less strongly than DMMP but more strongly than water, thus leading to a response to DMMP but not water. This example demonstrates how the choice of mesogen plays a central role in the performance of a LC chemical sensor. Many designs of mesogens that incorporate other metal cation binding functional groups can be envisaged but have not yet been explored.

In addition to the critical task of designing LC-solid interfaces in LC sensors, another largely untouched challenge is the design of the LC-air interface of the sensor. In the majority of past studies of LC sensors, in which a micrometer-thick film of LC was supported on a chemically functionalized surface (e.g., in a microwell or stabilized by arrays of micropillars), the LCs exhibited a perpendicular orientation at the upper free surface (to air) [19, 25, 29]. Manipulation of this orientation is an important design variable, however, because it can impact the change in elastic energy of the LC film that accompanies the LC response to a chemical species. So far, little work has been reported on the topic, but the importance of it in LC sensor design is illustrated by one recent example. In this example, LCs containing the cyclohexyl group (PCH series) were used [22]. For reasons that are not yet fully understood, these LCs exhibit planar anchoring at a free surface (interface to air) while maintaining a homeotropic orientation at a surface presenting metal cations (the latter through a coordination interaction between the nitrile groups of the PCH mesogens and metal cations). Importantly, it was demonstrated that this combination of interfacial ordering—planar anchoring at the free surface and homeotropic anchoring at the metal-cation-decorated surface—led to designs of LC sensors that exhibited faster responses and greater sensitivities to DMMP, as compared to LCs that adopt perpendicular orientations at free surfaces (5CB, E7 and others, Figure 2b)[22].When using a mixture of PCH3/PCH5, in contrast to 5CB, the LC is initially strained by hybrid anchoring with an elastic free energy per unit area of K/h, where K is the elastic constant of the LC and h is the LC film thickness. To trigger a response to DMMP, the only requirement is that the homeotropic anchoring strength be reduced to a value that is less than K/h ($\approx 10^{-5}$ J m^{-2}). In contrast, for nematic 5CB with an initially homeotropic state, exposure to DMMP must trigger a change in the orientation of the easy axis of the LC in order to generate an optical response. As a result, as shown by inspection of Figure 2b, gas phase concentrations of DMMP as low as 100 ppb can be detected with PCH3/PCH5; under the same conditions, 5CB generates no measurable response. For 1 ppm and 10 ppm DMMP, PCH3/PCH5 exhibited faster responses than observed when using 5CB.

Achieving Higher Chemical Specificity and Sensitivity in LC sensors by using Machine Learning. The strategies described above for design of LC chemical sensors focused on identification and optimization of the chemistry of mesogens and surfaces. A complementary strategy is to look for specificity in the response of LC systems to targeted chemical species by increasing the sophistication with which the spatial and temporal responses of LC systems are characterized. It is this "pattern recognition" approach that forms the basis of the aspect of the LC sensor design strategy that we discuss in this section. As detailed below, the approach is enabled by the availability and dissemination of machine-learning approaches. The term "machine learning" (ML) is attributed to an article [30] where the possibility of teaching a computer to learn how to play the game of checkers was demonstrated. In the past decade, the growth in computing power and availability of large datasets has elevated the importance of ML in most areas of science and engineering [31].

The first report of the use of ML in the context of LC sensors demonstrated that machine recognition of operator-specified features of the optical response of a LC sensor could be used to classify the response and thus improve the specificity and speed of a LC-based chemical sensor [32]. A range of different features were used to train the classifiers of the ML framework, including the average intensity of RGB channels of an image. The optical responses of surface-based LC sensors to either water vapor or DMMP were processed using two different training strategies, namely, dynamic and static training. The dynamic strategy trained a classifier (using a "training dataset" of images using average RGB feature information that was accumulated during the evolution of the LC response. The strategy was motivated by the observation that, for the experimental dataset under consideration, LC responses to water vapor tended to be slower than responses to DMMP. Therefore, the authors argued that the shape of the dynamic profiles of the RGB channels should provide valuable information to perform classification. However, the dynamic responses, as presented in Figure 3a, were found to exhibit variability from sample to sample. A *static* strategy was then explored based on classifying LC responses using spatial features in the images (independent of when they were obtained). This strategy was based on the hypothesis that subtle differences in spatial patterns (that are not obvious to the human eye) would be sufficient to distinguish between water vapor and DMMP. The static strategy has the key practical advantage that it does not require running a lengthy experiment to conduct classification, thus accelerating

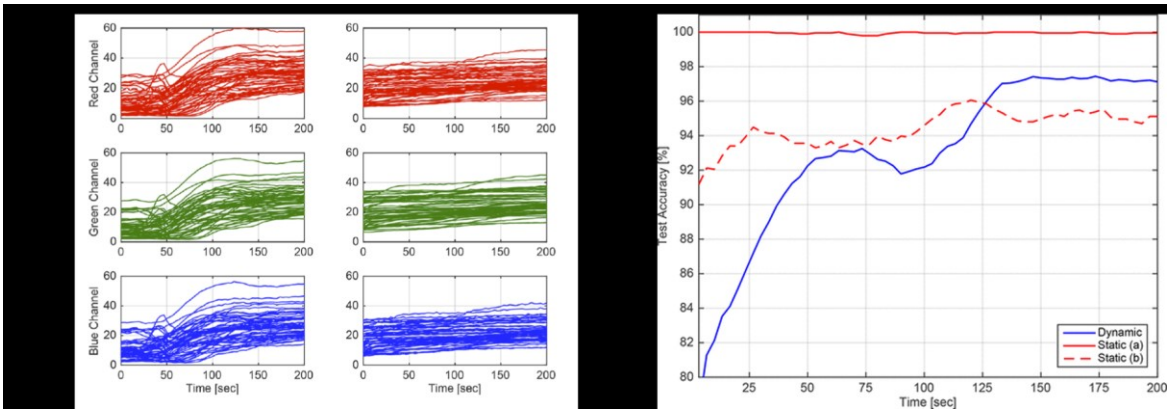

Figure 3. (a) Dynamic evolution of average red (top), green (middle), and blue (bottom) intensities of LC sensors responding to DMMP (left) and N_2-water (right). Each line represents a different sample (b) Average classification accuracy (for test set) achieved using ML approaches based on dynamic and static strategies. From Reference[32].

the speed of classification. As shown in Figure 3b, prediction accuracies of 99% were achieved by using images that were captured within only 3.3 s of tracking the LC response. The results demonstrate the potential utility of ML-based methods for distinguishing responses of LCs to chemical targets that are otherwise indistinguishable to human observers.

A second study that has used ML methods to analyze LC sensor responses employed convolutional neural networks (CNN) [33]. Most implementations of CNNs are inspired by the deep neural network model (AlexNet) of Krizhevsky *et al*. that was reported in 2012 [34]. AlexNet was trained using millions of images found on the Internet, thus mimicking how humans categorize new objects based on prior information. In the context of research involving LCs, AlexNet-based frameworks have been used to identify LC phases and predict the order parameter of simulated nematic LCs [35, 36]. CNNs have also been shown to identify the pitch length of simulated samples of cholesteric LCs [35].

CNNs perform two major tasks, feature extraction (red box in Figure 4a) and classification (blue box in Figure 4a)[37]. Feature extraction is performed by so-called "convolution", in which an operation is performed on an input image using a filter. The filter, which is a small matrix, acts as a "keyhole" with which the image is viewed: as the image is scanned, a mathematical operation (defined by the matrix that comprises the filter) is performed on the local part of the image (as seen through the keyhole). The output of the convolution is a so-called feature image, which is a small set of numerical values that can be used to summarize and classify the features in an image (a feature image is created for each filter). An example of applying a convolution filter to an image is illustrated in Figure 4c. Different filters report on the presence of different patterns in the image. The larger the value of the filter output, the more similar the given neighborhood is to the pattern that the filter is attempting to find. The pooling step shown in Figure 4a typically aims to reduce the dimensionality of the feature image by selecting extreme values of the feature image ("max pooling"). Subsequent convolutions compress the feature images to the point where a decision (e.g., classification or regression) can be made. This part of the CNN is termed a fully connected layer. During training of the CNN, there is a backpropagation step in which filters are selected to maximize the accuracy of the output classification.

VGG16, (a more compact CNN than Alexnet) was used to analyze color micrographs of LC sensor optical responses [33]. The study led to the conclusion that the CNN learned that the hue distributions (color spatial patterns) provided informative set of features that can be used to characterize LC sensor responses. As importantly, the extracted features were connected to physical characteristics of the LC responses to the chemical targets. In particular, the hue identified by the CNN to be important in classification of the LC response reflects the different orientations of the LCs within the film (interference colors generated by the white light illumination). As shown in Figure 4d and 4e, the maximally activating textures reveal that DMMP and water are characterized by a distinct set of hues (reflecting differences in orientation of the LC). For the sensor reported above that gave a visible optical response to both water and DMMP (increase in brightness when observed with the naked eye), the CNN was able to classify the micrographs of LC responses to water and DMMP

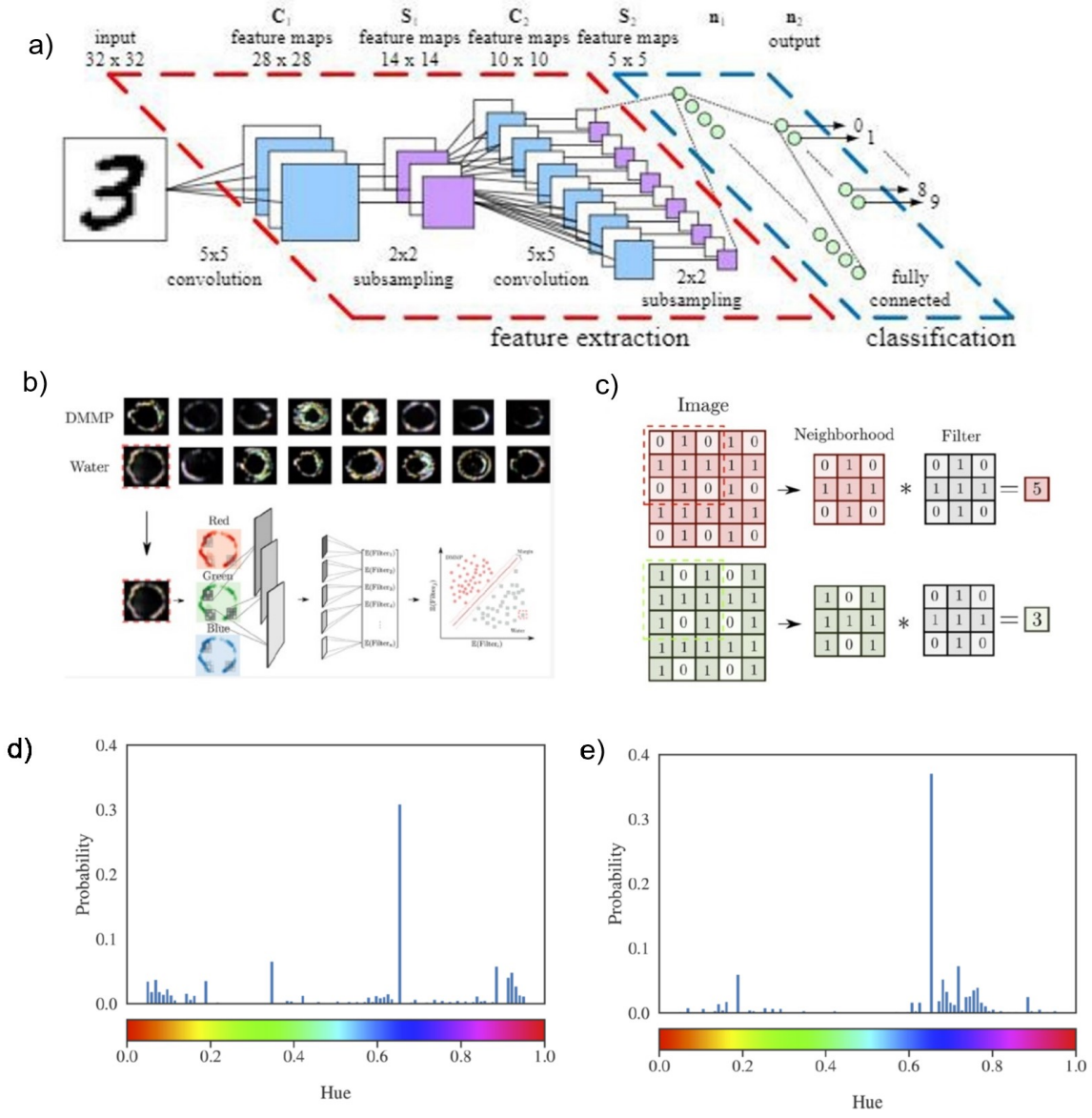

Figure 4. (a) An example of a typical CNN architecture (b) Schematic illustration of feature extraction and classification framework for analysis of LC sensor responses using ML approaches (c) Illustration of the application of a convolution filter to two different images (d) Hue distributions that characterize the response of LC sensors to water or (e) DMMP, as identified using a CNN. From references[32-34].

with 100% accuracy (i.e., it could distinguish between DMMP and water). Similar to the first ML study of LC sensors, the results of this second study indicate that LC features developed early in the sensor response (first 30 s) are highly informative and sufficient to discriminate between chemical environments.

Strategies for Design of LC Chemical Sensors that do not Rely on Responsive Surfaces. The examples of LC sensor design that were discussed above rely on the use of surfaces to achieve chemical selectivity (i.e., they are based on surface anchoring transitions). An alternative strategy is to design LC systems that undergo changes in bulk phase organization in response to exposure to targeted chemical species. While this strategy has a long history, starting with the use of phase

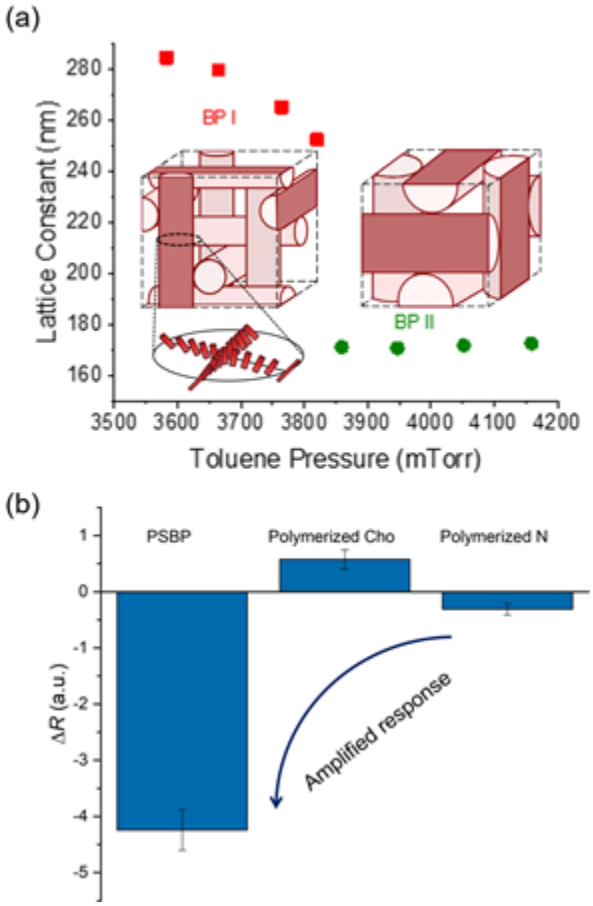

Figure 5. (a) Change of lattice spacing of a BP (BPI and BPII) LC exposed to toluene vapor. Inserts show the corresponding structures of BPI and BPII. (b) Optical response of either a polymer-stabilized BP, polymerized cholesteric and polymerized nematic sample to toluene vapor at 930 ± 70 ppm. From Reference[39, 45, 48].

transitions induced by absorption of volatile organic compounds (VOCs), as detailed below, more recent efforts have turned to the use of chiral LC phases, including cholesteric and blue phase (BP) LCs, and the design of chemically-selective chiral dopants.

Chiral LC phases are promising for sensing applications due to their intrinsic optical properties, such as Brag reflection (Figure 5). A number of past studies demonstrate that chiral LCs exhibit measurable optical responses when volatile organic compounds absorb into them [4, 9, 38-43]. For example, cholesteric phases have been demonstrated to respond to tetrachloroethylene, with the response arising from an expansion of the pitch of the cholesteric phase [42]. More recent studies have extended investigations of chiral LC phases for VOC sensing to BPs, including BPI (body

center cubic) and BPII (simple cubic) phases (Figure 5a)). Interestingly, when exposed to toluene vapor, the lattice expands in BPI while it shrinks in BPII, revealing that the influence of the toluene on the BP is not simply to swell the material, as occurs with cholesteric LCs. Polymerized BPs, which exhibit stable BP phases over a wide range of temperatures [9, 38, 39], have also been explored for VOC sensing. Inspection of Figure 6b reveals that a polymer-stabilized BP can generate a larger optical response to toluene vapor than either a polymerized cholesteric or nematic phase. Overall, polymerized LC phases appear promising for design of LC sensors, in part because they are self-supporting and thus easy to integrate into devices.

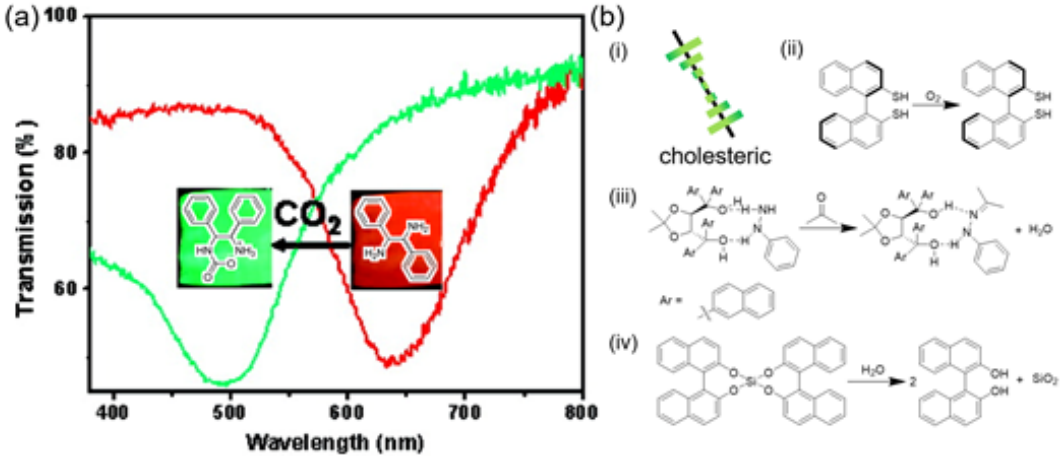

Figure 6. Cholesteric LC sensors doped with reactive chiral dopants: (a) Transmission spectra of cholesteric LC film containing a chiral dopant that reacts with CO_2, before (red) and after (green) exposure to CO_2. Insert shows the images of the cholesteric film before (red) and after (green) exposure to CO_2 for 1 h, and the corresponding reaction between the doped reactive chiral dopant and CO_2. (b) (i) Schematic illustration of the structure of the cholesteric LC (half pitch), (ii-iv) Molecular structures of various chiral dopants and their corresponding reactions with (ii) O_2, (iii) acetone, (iv) water. From references[15, 45.]

A particularly interesting approach based on cholesteric LCs involves the use of chiral dopants that undergo changes in helical twisting power in the presence of targeted chemical species (via physical or chemical interactions) [15, 44-48]. For example, Figure 6a shows the response of a cholesteric film doped with a chiral diamine (Figure 6a insert) upon exposure to CO_2 [15]. Because the chiral diamine itself has a low helical twisting power, a TADDOL derivative with a high helical twisting power was also introduced into the LC. The TADDOL derivative formed a complex with the diamine and enabled Bragg reflection of the film in the visible region. Initially, the cholesteric film exhibited a red color with maximum reflection at 637 nm. Upon transformation of the diamine to a carbamate (Figure 6a insert) via reaction with CO_2, the helical twisting power increased due to dissociation of the complex. This change generated a greenish blue appearance and a maximum in reflectance at 495 nm. Beyond the use of reactive diamine dopants for CO_2 detection, Figure

5(b, ii-iv) shows reactive chiral dopants that have been reported to form cholesteric phases that respond to O_2, acetone vapor, and humidity[9, 14, 15, 39, 40, 42, 46].

Beyond Equilibrium: Design of Biological Sensors based on Non-Equilibrium Interfacial Phenomena In addition to efforts to create LC sensors that detect the presence of targeted chemical species present in the gas phase, a substantial number of studies have reported LC sensors for detection of biological species from aqueous phases. In these examples, a thermotropic LC is brought into contact with an aqueous phase, and interfacial phenomena at the LC-aqueous interface leads to changes in the ordering of LCs. For example, a range of past studies using LC sensors with LC-aqueous interfaces have reported observations of orientational transitions of LCs triggered by the adsorption or reorganization of amphiphilic molecules at the interface [16, 49-52]. These changes in orientation of the LCs reflect, in part, the interaction of LC mesogens with aliphatic tails of the amphiphiles and depend on the structure and concentration of the amphiphiles [13, 17, 51, 53] as well as the solution conditions [23].

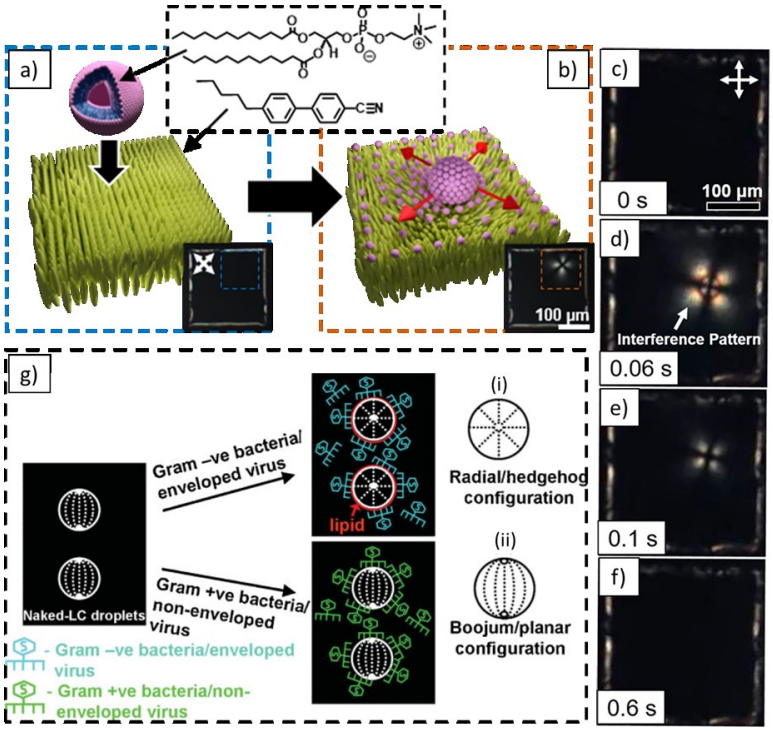

Figure 7. Schematic illustrations of (a) a vesicle approaching a LC-aqueous interface [inset, top: structures of DLPC and 5CB; bottom: polarized light micrograph (crossed polarizers) of the sample showing a dark texture] and (b) a vesicle colliding with the interface and subsequently spreading along the interface [inset, polarized light micrograph (crossed polarizers) showing a "blink"]. (c-f) Sequential micrographs of a single blinking event. (g) Schematic representation of the interaction of viruses or bacteria with LC emulsions. The cartoons depict the i) radial and ii) bipolar configurations of LC droplets. From references [54, 55].

Whereas the majority of past efforts to develop biomolecular sensors at LC-aqueous interfaces have focused on driving the LC between two equilibrium states (with or without the target), recent studies highlight the opportunity to create LC sensors that operate beyond equilibrium. To illustrate the approach, we describe recent observations of non-equilibrium behaviors of LC interfaces that are incubated against aqueous dispersions of amphiphilic assemblies[54]. In these studies, the LCs (e.g., nematic phases of 5CB) were observed to generate spatially localized and transient flashes of light when viewed through crossed polarizers. It was deduced that amphiphilic assemblies of

phospholipids (vesicles of DLPC, Figure 7a)) collided with the LC-aqueous interface, and that subsequent spreading of the amphiphiles across the interface (Figure 7b) generated a transient surface tension gradient and associated interfacial flow (Marangoni flow). The surface flow is sufficiently strong to realign the LC near the interface and generate an optical response (a "blink") (Figure 7c-f). Experimental observations revealed a first order relationship between the concentration of vesicles in the aqueous phase and the frequency of blinking, consistent with blinking events arising from the collisions of single vesicles with the LC interface.

The above-described study hints at a range of future directions of exploration involving lipidic assemblies at LC interfaces. For example, past studies have reported that the transfer of lipid onto LC interfaces from bacteria [55] and viruses [55-57] can trigger LC ordering transitions (Figure 7g). Specifically, micrometer-sized droplets of nematic 5CB transition from bipolar (planar) to radial (hedgehog) configurations when contacted with Gram-negative bacteria (E. *coli*) or lipid-enveloped viruses (A/NWS/Tokyo/67), but not when contacted with Gram-positive bacteria (*Bacillus subtilis*) or non-enveloped viruses (M13 helper phage) (Figure 7g). These observations are consistent with the transfer of lipids from the surfaces of Gram-negative bacteria and lipid-enveloped viruses to the interfaces of the LC droplets. When combined with the observation that single amphiphilic vesicles can trigger non-equilibrium states, it also appears likely that highly sensitive methods of detection of vesicles, viruses and bacteria may be possible using LCs driven beyond equilibrium.

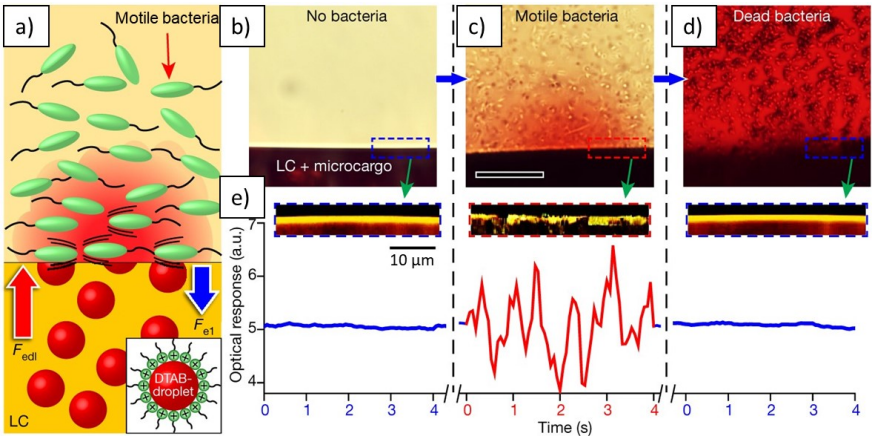

Figure 8. (a) Schematic illustration (side view) and (b–d) sequential micrographs (side view) showing interfacial shear stresses generated by motile bacteria (*E. coli*) triggering the self-regulated release of microdroplets containing anti-bacterial agent (silver salts) and a red tracer, (b) before the arrival of bacteria, (c) immediately after the arrival of motile bacteria and (d) two hours after the arrival of bacteria and following cell death. (e) Optical responses and side views of the LC interface corresponding to (b–d). From reference[58].

A second example of the use of non-equilibrium interfacial states of LCs for biological sensing revolves around the hydrodynamic interactions of motile bacteria with the aqueous interfaces of LC systems[58]. Specifically, it was shown that the hydrodynamic shear stresses transmitted from motile bacteria onto LC interfaces are sufficient to drive the reorientation of LCs and thus generate an optical response that reflects the motion of the bacteria. In addition, it was reported that aqueous micrometer-sized droplets, initially trapped within the LCs, could be released from the LC by mechanical shear stress generated by the swimming motion of bacteria (*E. coli*). When the aqueous microdroplets contained antibacterial agents (silver salts), the release of the microdroplets

in the presence of motile bacteria resulted in bacterial cell death, thus generating a self-regulated release of antimicrobial agent. Here we emphasize that the antibacterial agent is only released in the presence of the shear stress generated by motile bacteria, and that it functions in a feedback loop, stopping the release of antibacterial agents as the trigger is eliminated (Figure 8b-d). The self-regulating behavior of the LC system suggests that LCs not only offer the basis of promising biological sensors, but that they can integrate the functions of actuators to provide stimuli dependent release of active agents (e.g., to avoid release of antibacterial agent in the absence of motile bacteria).

Concluding statements

This article describes areas of opportunity related to the design of LC-based chemical and biological sensors with a focus on four broad messages:

First, there exist a range of surface-based strategies for design of LC sensors, employing metal-ligand interactions, redox-reactions and noble metal surfaces. In each of these contexts, there remain many opportunities to develop new alignment chemistries and new mesogen designs[19-22, 27]. To date, existing strategies have largely relied on the menu of LCs developed for electrooptical applications. The design of LCs with properties tailored for LC sensors is almost untouched.

Second, the design and analysis of LC sensors is being increasingly enabled by computational methods. As illustrated by examples given in this article, computational methods include electronic structure calculations for screening of chemical functional groups for incorporation into LC dopants, mesogen designs and to present from surfaces. Additionally, ML approaches are proving useful in identifying subtle spatial and temporal features of LC optical responses to chemical and biological targets, thus decreasing the reliance of tailored chemistry to achieve specificity in the operation of the LC sensor. Both classes of approaches appear fertile territory for advancing LC sensor design[32, 33].

Third, a promising strategy for design of LC chemical sensors revolves around the use of chiral dopants with helical twisting power that changes upon interaction/reaction with targeted chemical species. Polymerized blue phases appear useful hosts for such reactive chiral dopants, as they are self-supporting, stable over a wide range of temperatures, and subtle changes in organization can be reported via changes in Bragg diffraction[15, 38, 43, 46, 59].

Fourth, and finally, this article highlights the opportunity to perform sensing functions using LCs that are driven into non-equilibrium states. It has long been known that LCs undergo shear alignment, but recent studies demonstrate that shear stresses encountered in living biological systems or generated by gradients in interfacial concentration of amphiphiles, are sufficient to triggered optical and other functional responses of LCs (e.g., release of microcargo). The complex dynamic responses of LC to non-equilibrium states offers a range of pathways towards adaptive and self-regulating chemical systems, where the responses to multiple stimuli are computed by the LC thus giving rise to a level of autonomy and function that is increasingly similar to living biological systems (e.g., function of a biological membrane)[54, 58].

References

1. Bellini, T.; Zanchetta, G.; Fraccia, T. P.; Cerbino, R.; Tsai, E.; Smith, G. P.; Moran, M. J.; Walba, D. M.; Clark, N. A. *Proc Natl Acad Sci U S A* **2012,** 109, (4), 1110-1115.
2. Brown, G. H.; Wolken, J. J., Chapter 5 - The Structural Molecules of Life. In *Liquid Crystals and Biological Structures*, Brown, G. H.; Wolken, J. J., Eds. Academic Press: 1979; pp 56-72.
3. Kawamoto, H. *Proceedings of the IEEE* **2002,** 90, (4), 460-500.
4. Poziomek, E. J.; Novak, T. J.; Mackay, R. A. *Molecular Crystals and Liquid Crystals* **1974,** 27, (1-2), 175-185.
5. Champa, R. A., Heterocyclic Liquid Crystals and Some Air Force Applications of Mesomorphic Compounds. In *Liquid Crystals and Ordered Fluids: Volume 2*, Johnson, J. F.; Porter, R. S., Eds. Springer US: Boston, MA, 1974; pp 507-514.
6. Bocharov, Y. V.; Gurova, I. N.; Kapustina, O. A.; Remizova, E. I.; Reshetov, V. N.; Grigoriev, S. A.; Demianovich, M. V.; Novikov, V. N. *Sensors and Actuators A: Physical* **1991,** 28, (3), 179-183.
7. Parmar, D. S.; Singh, J. J. *Applied Physics Letters* **1992,** 61, (17), 2039-2041.
8. Anagni, F.; Bartoletti, C.; Marchetti, U.; Podesta, L.; Sacerdoti, G. *IEEE Transactions on Instrumentation and Measurement* **1994,** 43, (3), 475-480.
9. Dickert, F. L.; Haunschild, A.; Hofmann, P. *Fresenius' Journal of Analytical Chemistry* **1994,** 350, (10), 577-581.
10. Gupta, V. K.; Skaife, J. J.; Dubrovsky, T. B.; Abbott, N. L. *Science* **1998,** 279, (5359), 2077.
11. Balasubramaniam, V. M.; Sastry, S. K. *Journal of Food Engineering* **1995,** 26, (2), 219-230.
12. Shah, R. R.; Abbott, N. L. *Science* **2001,** 293, (5533), 1296.
13. Lowe, A. M.; Abbott, N. L. *Chem Mater* **2012,** 24, (5), 746-758.
14. Parmar, D. S. *Review of Scientific Instruments* **1991,** 62, (6), 1596-1608.
15. Han, Y.; Pacheco, K.; Bastiaansen, C. W. M.; Broer, D. J.; Sijbesma, R. P. *Journal of the American Chemical Society* **2010,** 132, (9), 2961-2967.
16. Brake, J. M.; Daschner, M. K.; Luk, Y. Y.; Abbott, N. L. *Science* **2003,** 302, (5653), 2094-7.
17. Carlton, R. J.; Hunter, J. T.; Miller, D. S.; Abbasi, R.; Mushenheim, P. C.; Tan, L. N.; Abbott, N. L. *Liq Cryst Rev* **2013,** 1, (1), 29-51.
18. Roling, L. T.; Scaranto, J.; Herron, J. A.; Yu, H.; Choi, S.; Abbott, N. L.; Mavrikakis, M. *Nature Communications* **2016,** 7, (1), 13338.
19. Szilvási, T.; Bao, N.; Nayani, K.; Yu, H.; Rai, P.; Twieg, R. J.; Mavrikakis, M.; Abbott, N. L. *Angewandte Chemie International Edition* **2018,** 57, (31), 9665-9669.
20. Szilvási, T.; Roling, L. T.; Yu, H.; Rai, P.; Choi, S.; Twieg, R. J.; Mavrikakis, M.; Abbott, N. L. *Chemistry of Materials* **2017,** 29, (8), 3563-3571.
21. Yu, H.; Szilvási, T.; Wang, K.; Gold, J. I.; Bao, N.; Twieg, R. J.; Mavrikakis, M.; Abbott, N. L. *Journal of the American Chemical Society* **2019,** 141, (40), 16003-16013.
22. Nayani, K.; Rai, P.; Bao, N.; Yu, H.; Mavrikakis, M.; Twieg, R. J.; Abbott, N. L. *Advanced Materials* **2018,** 30, (27), 1706707.
23. Brake, J. M.; Abbott, N. L. *Langmuir* **2007,** 23, (16), 8497-507.
24. Jerome, B. *Reports on Progress in Physics* **1991,** 54, (3), 391-451.
25. Hunter, J. T.; Abbott, N. L. *ACS Applied Materials & Interfaces* **2014,** 6, (4), 2362-2369.
26. Cadwell, K. D.; Alf, M. E.; Abbott, N. L. *The Journal of Physical Chemistry B* **2006,** 110, (51), 26081-26088.
27. Yu, H.; Szilvási, T.; Rai, P.; Twieg, R. J.; Mavrikakis, M.; Abbott, N. L. *Advanced Functional Materials* **2018,** 28, (13), 1703581.
28. Schwarz, D.; van Gastel, R.; Zandvliet, H. J. W.; Poelsema, B. *The Journal of Physical Chemistry C* **2013,** 117, (2), 1020-1029.

29. Sadati, M.; Ramezani-Dakhel, H.; Bu, W.; Sevgen, E.; Liang, Z.; Erol, C.; Rahimi, M.; Taheri Qazvini, N.; Lin, B.; Abbott, N. L.; Roux, B. t.; Schlossman, M. L.; de Pablo, J. J. *Journal of the American Chemical Society* **2017,** 139, (10), 3841-3850.
30. Samuel, A. L. *IBM Journal of Research and Development* **2000,** 44, (1.2), 206-226.
31. Jackson, N. E.; Webb, M. A.; de Pablo, J. J. *Current Opinion in Chemical Engineering* **2019,** 23, 106-114.
32. Cao, Y.; Yu, H.; Abbott, N. L.; Zavala, V. M. *ACS Sensors* **2018,** 3, (11), 2237-2245.
33. Smith, A. D.; Abbott, N.; Zavala, V. M. *The Journal of Physical Chemistry C* **2020,** 124, (28), 15152-15161.
34. Blanc-Talon, J.; Kleihorst, R.; Philips, W.; Popescu, D.; Scheunders, P., *Advanced Concepts for Intelligent Vision Systems: 13th International Conference, ACIVS 2011, Ghent, Belgium, August 22-25, 2011. Proceedings*. 2011.
35. Sigaki, H. Y. D.; de Souza, R. F.; de Souza, R. T.; Zola, R. S.; Ribeiro, H. V. *Physical Review E* **2019,** 99, (1), 013311.
36. Sigaki, H. Y. D.; Lenzi, E. K.; Zola, R. S.; Perc, M.; Ribeiro, H. V. *Scientific Reports* **2020,** 10, (1), 7664.
37. Peemen M., M. B., Corporaal H. *Advanced Concepts for Intelligent Vision Systems. ACIVS 2011.* **2011,** 6915, (Advanced Concepts for Intelligent Vision Systems. ACIVS 2011. Lecture Notes in Computer Science, vol 6915. Springer, Berlin, Heidelberg.
38. Bedolla Pantoja, M. A.; Yang, Y.; Abbott, N. L. *Liquid Crystals* **2019,** 46, (13-14), 1925-1936.
39. Chang, C.-K.; Kuo, H.-L.; Tang, K.-T.; Chiu, S.-W. *Applied Physics Letters* **2011,** 99, (7), 073504.
40. Mujahid, A.; Stathopulos, H.; Lieberzeit, P. A.; Dickert, F. L. *Sensors (Basel, Switzerland)* **2010,** 10, (5), 4887-4897.
41. Sutarlie, L.; Qin, H.; Yang, K.-L. *Analyst* **2010,** 135, (7), 1691-1696.
42. Winterbottom, D. A.; Narayanaswamy, R.; Raimundo, I. M. *Sensors and Actuators B: Chemical* **2003,** 90, (1), 52-57.
43. Yang, Y.; Kim, Y.-K.; Wang, X.; Tsuei, M.; Abbott, N. L. *ACS Applied Materials & Interfaces* **2020**.
44. Cachelin, P.; Green, J. P.; Peijs, T.; Heeney, M.; Bastiaansen, C. W. M. *Advanced Optical Materials* **2016,** 4, (4), 592-596.
45. Pschyklenk, L.; Wagner, T.; Lorenz, A.; Kaul, P. *ACS Applied Polymer Materials* **2020,** 2, (5), 1925-1932.
46. Saha, A.; Tanaka, Y.; Han, Y.; Bastiaansen, C. M. W.; Broer, D. J.; Sijbesma, R. P. *Chemical Communications* **2012,** 48, (38), 4579-4581.
47. Su, X.; Voskian, S.; Hughes, R. P.; Aprahamian, I. *Angewandte Chemie International Edition* **2013,** 52, (41), 10734-10739.
48. Tokunaga, S.; Itoh, Y.; Tanaka, H.; Araoka, F.; Aida, T. *Journal of the American Chemical Society* **2018,** 140, (35), 10946-10949.
49. Price, A. D.; Schwartz, D. K. *J Phys Chem B* **2007,** 111, (5), 1007-15.
50. Gupta, J. K.; Abbott, N. L. *Langmuir* **2009,** 25, (4), 2026-33.
51. Lockwood, N. A.; de Pablo, J. J.; Abbott, N. L. *Langmuir* **2005,** 21, (15), 6805-14.
52. Tian, T.; Kang, Q.; Wang, T.; Xiao, J.; Yu, L. *J Colloid Interface Sci* **2018,** 518, 111-121.
53. Badami, J. V.; Bernstein, C.; Maldarelli, C.; Tu, R. S. *Soft Matter* **2015,** 11, (33), 6604-12.
54. Tsuei, M.; Shivrayan, M.; Kim, Y. K.; Thayumanavan, S.; Abbott, N. L. *J Am Chem Soc* **2020,** 142, (13), 6139-6148.
55. Sivakumar, S. W., K. M.; Gupta, J. K.; Abbott, N. L.; Caruso F. *Advanced Functional Materials* **2009,** 19, 2260-2265.
56. Espinoza, L. A.; Schumann, K. R.; Luk, Y. Y.; Israel, B. A.; Abbott, N. L. *Langmuir* **2004,** 20, (6), 2375-85.
57. Jang, C. H.; Cheng, L. L.; Olsen, C. W.; Abbott, N. L. *Nano Lett* **2006,** 6, (5), 1053-8.
58. Kim, Y. K.; Wang, X.; Mondkar, P.; Bukusoglu, E.; Abbott, N. L. *Nature* **2018,** 557, (7706), 539-544.
59. Wolarz, E.; Moryson, H.; Bauman, D. *Displays* **1992,** 13, (4), 171-178.